Supporting information

Ultrathin nickel hydroxide on carbon coated 3D-porous copper structures for high performance supercapacitors

Kyeong-Nam Kang[a], Ik-Hee Kim[a], Ananthakumar Ramadoss[b], Sun-I Kim[a], Jong-Chul Yoon[a], and Ji-Hyun Jang*[a]

[a]School of Energy Chemical Engineering, Low Dimensional Carbon Materials center, Ulsan National Institute of Science and Technology, Ulsan 689-798, Republic of Korea. E-mail: clau@unist.ac.kr; Fax: +82-52-217-3008; Tel; +82-52-217-2922

[b]Mixed Siganl Integrated Circuit Lab, School of Electrical Engineering, Korea Advanced Institute of Science and Technology, Daejeon 305-701, Republic of Korea.

Section 1. Calculation of specific capacitance value.

1-1. Specific capacitance with galvanostatic discharge curves

We can calculate the capacitance value depending on the current density by selecting the dV/dt once we know the exact discharge time, potential range, and current density.

$$C_s = \frac{i}{m\,(\Delta V / \Delta t)}$$

- ✓ C → specific capacitance
- ✓ m → mass of active material
- ✓ ΔV → window range
- ✓ Δt→ discharge time
- ✓ i → current density

$$C = \frac{(0.4 \times 10^{-3}\ \mathrm{A})}{(0.4 \times 10^{-3}\ \mathrm{g})(0.729 - 0.0)/(1356.5\ \mathrm{s})} = \frac{1\ A/g}{(0.729-0.0)/(1356.5\ \mathrm{s})} = 1860.0\ F/g$$

$$C = \frac{(0.8 \times 10^{-3}\ \mathrm{A})}{(0.4 \times 10^{-3}\ \mathrm{g}) \times (0.743-0.0)/(683.2\ \mathrm{s})} = \frac{2\ A/g}{(0.743 - 0.0)/(683.2\ \mathrm{s})} = 1839.2\ F/g$$

$$C = \frac{(2 \times 10^{-3}\ \mathrm{A})}{(0.4 \times 10^{-3}\ \mathrm{g}) \times (0.75 -0.0)/(272.7\ \mathrm{s})} = \frac{5\ A/g}{(0.75 - 0.0)/(272.7\ \mathrm{s})} = 1818.8\ F/g$$

$$C=\frac{(4\times10^{-3}\ \mathrm{A})}{(0.4\times10^{-3}\ \mathrm{g})\times(0.753-0.0)/(133.1\ \mathrm{s})}=\frac{10\ A/g}{(0.753-0.0)/(133.1\ \mathrm{s})}=\ 1768.6\ F/g$$

$$C=\frac{(8\times10^{-3}\ \mathrm{A})}{(0.4\times10^{-3}\ \mathrm{g})\times(0.752-0.0)/(64.5\ \mathrm{s})}=\frac{20\ A/g}{(0.752-0.0)/(64.5\ \mathrm{s})}=\ 1715.9\ F/g$$

$$C=\frac{(20\times10^{-3}\ \mathrm{A})}{(0.4\times10^{-3}\ \mathrm{g})\times(0.744-0.0)/(23.9\ \mathrm{s})}=\frac{50\ A/g}{(0.744-0.0)/(23.9\ \mathrm{s})}=\ 1605.8\ F/g$$

1-2. Calculation of energy density and power density

$$\mathrm{E}=\frac{1}{2}C_tV^2$$

$$\mathrm{P}=\frac{E}{t}$$

Where C_t is the specific capacitance of the supercapacitor based on the total mass of the two electrodes (F/g), V is the potential window in the discharge process, and t is the discharge time(s). The calculated capacitance of the hybrid supercapacitor was,

$$C_t=\frac{(0.8\times10^{-3}\ \mathrm{A})}{(0.8\times10^{-3}\ \mathrm{g})(1.5-0.0)/(711.5\ \mathrm{s})}=\frac{1\ A/g}{(1.5-0.0)/(711.5\ \mathrm{s})}=\ 474.3\ F/g$$

$$\mathrm{E}=\frac{1}{2}(474.3)(1.5)^2\left(\frac{1000}{3600}\right)=147.9\ \frac{Wh}{kg},\ P=\frac{147.9}{711.5}(3600)=0.75\ \frac{kW}{kg}$$

$$C_t=\frac{(1.6\times10^{-3}\ \mathrm{A})}{(0.8\times10^{-3}\ \mathrm{g})(1.5-0.0)/(352.4\ \mathrm{s})}=\frac{2\ A/g}{(1.5-0.0)/(352.4\ \mathrm{s})}=\ 470.0\ F/g$$

$$\mathrm{E}=\frac{1}{2}(470.0)(1.5)^2\left(\frac{1000}{3600}\right)=146.9\ \frac{Wh}{kg},\ P=\frac{146.9}{352.4}(3600)=1.5\ \frac{kW}{kg}$$

$$C_t=\frac{(4.0\times10^{-3}\ \mathrm{A})}{(0.8\times10^{-3}\ \mathrm{g})(1.5-0.0)/(111.9\ \mathrm{s})}=\frac{5\ A/g}{(1.5-0.0)/(111.9\ \mathrm{s})}=\ 373.8\ F/g$$

$$\mathrm{E}=\frac{1}{2}(373.8)(1.5)^2\left(\frac{1000}{3600}\right)=116.8\ \frac{Wh}{kg},\ P=\frac{116.8}{111.9}(3600)=3.8\ \frac{kW}{kg}$$

$$C_t=\frac{(8\times10^{-3}\ \mathrm{A})}{(0.8\times10^{-3}\ \mathrm{g})(1.49-0.0)/(46.4\ \mathrm{s})}=\frac{10\ A/g}{(1.49-0.0)/(46.4\ \mathrm{s})}=\ 310.4\ F/g$$

$$\mathrm{E}=\frac{1}{2}(310.4)(1.49)^2\left(\frac{1000}{3600}\right)=97.0\ \frac{Wh}{kg},\ P=\frac{97.0}{46.4}(3600)=7.5\ \frac{kW}{kg}$$

$$C_t=\frac{(16\times10^{-3}\ \mathrm{A})}{(0.8\times10^{-3}\ \mathrm{g})(1.49-0.0)/(19.2\ \mathrm{s})}=\frac{20\ A/g}{(1.49-0.0)/(19.2\ \mathrm{s})}=\ 258.2\ F/g$$

$$\mathrm{E}=\frac{1}{2}(258.2)(1.49)^2\left(\frac{1000}{3600}\right)=80.8\ \frac{Wh}{kg},\ P=\frac{80.8}{19.2}(3600)=15.1\ \frac{kW}{kg}$$

$$C_t = \frac{(40\times10^{-3}\ \mathrm{A})}{(0.8\times10^{-3}\ \mathrm{g})(1.48 - 0.0)/(5.0\ \mathrm{s})} = \frac{50\ A/g}{(1.48\text{-}0.0)/(5.0\ \mathrm{s})} = 168.9\ F/g$$

$$\mathrm{E} = \frac{1}{2}(168.9)(1.48)^2\left(\frac{1000}{3600}\right) = 51.4\ \frac{Wh}{kg},\quad P = \frac{51.4}{5.0}(3600) = 37.0\ \frac{kW}{kg}$$

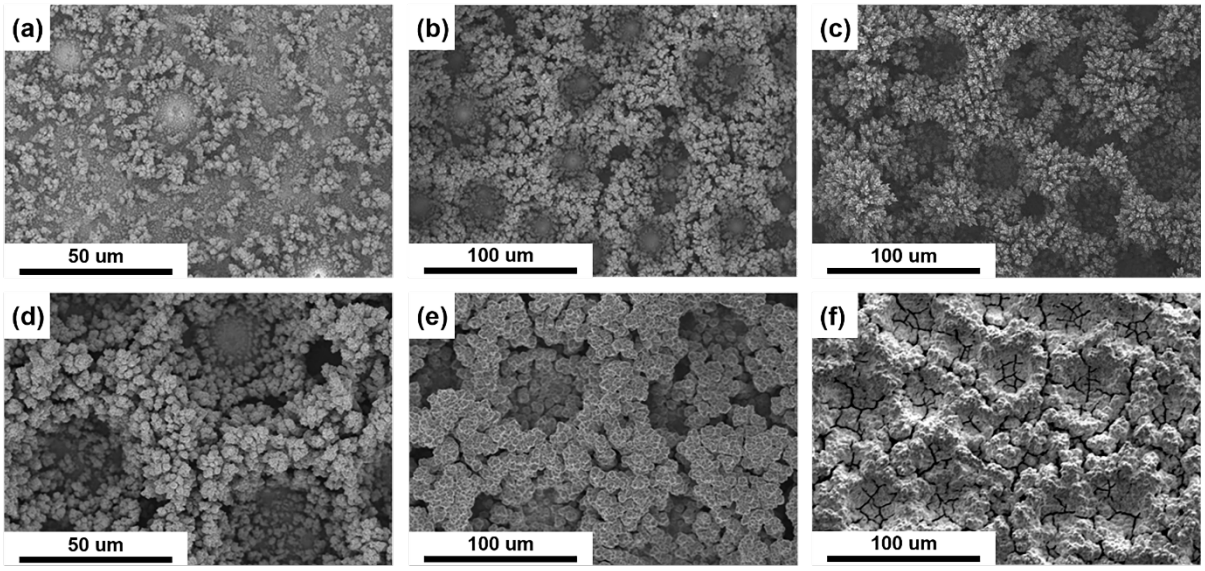

Figure S1. SEM images of the 3D-porous copper structure(3D-Cu) on the Ni film created by electrochemical deposition process, for different periods of time (a) 5 s, (b) 15 s, (c) 30 s, (d) 45 s, (e) 60 s, and (f) 90 s. The optimized deposition time was 30 s.

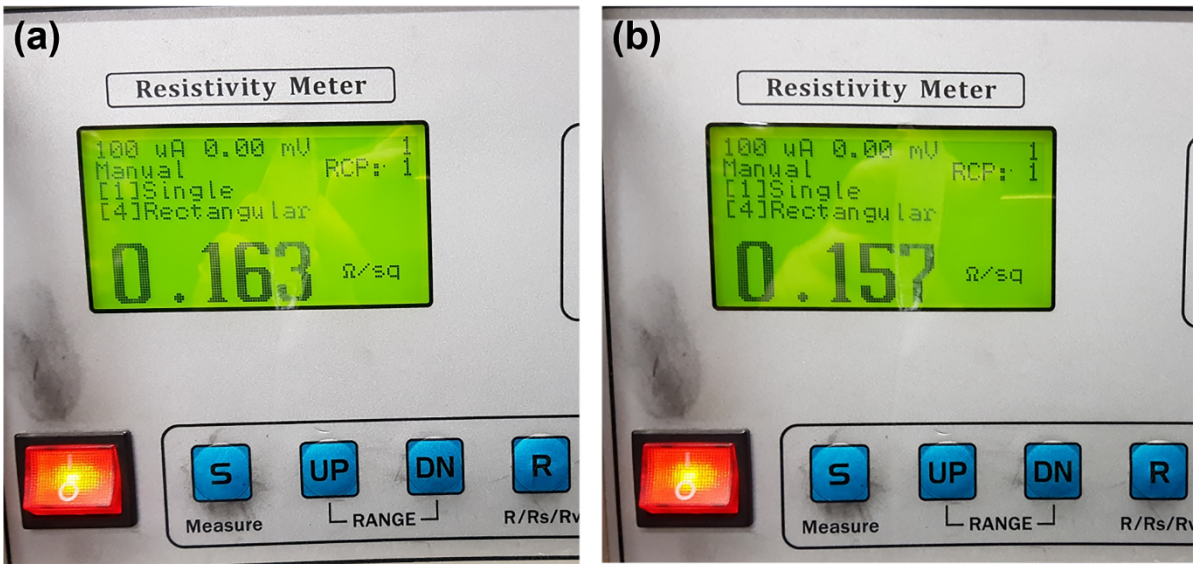

Figure S2. Conductivity measurement data by four-point probe resistivity meter (FPP-RS8, DASOL ENG) of 3D-Cu (left) and 3D-C/Cu (Right)

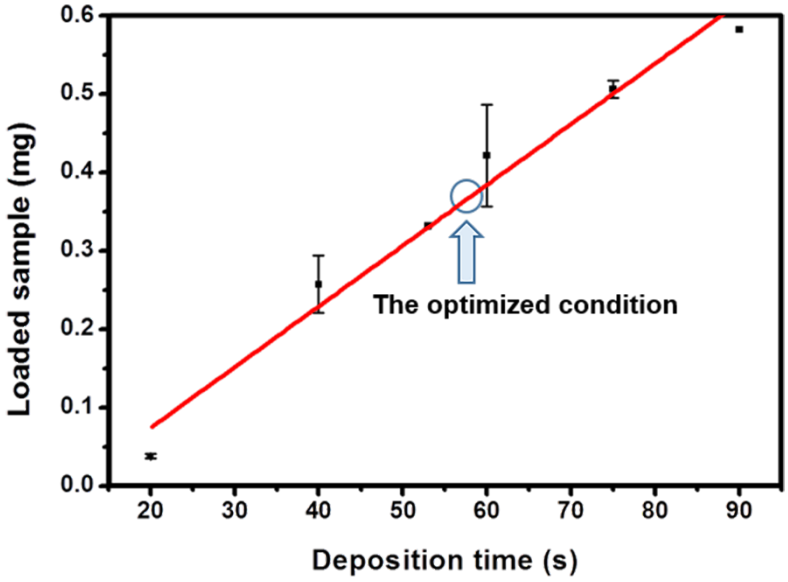

Figure S3. Loading amount of $Ni(OH)_2$ on 3D-Cu as a function of deposition time.

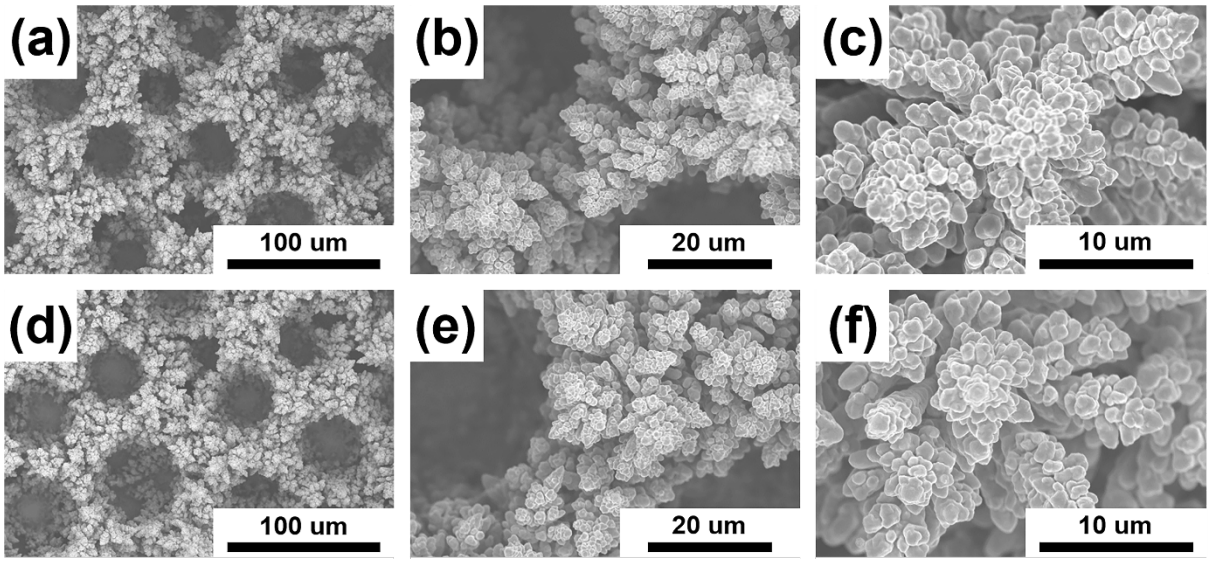

Figure S4. Comparison of SEM images of the 3D-Cu electrode (a-c) and 3D-C/Cu electrode (d-f) at various magnifications.

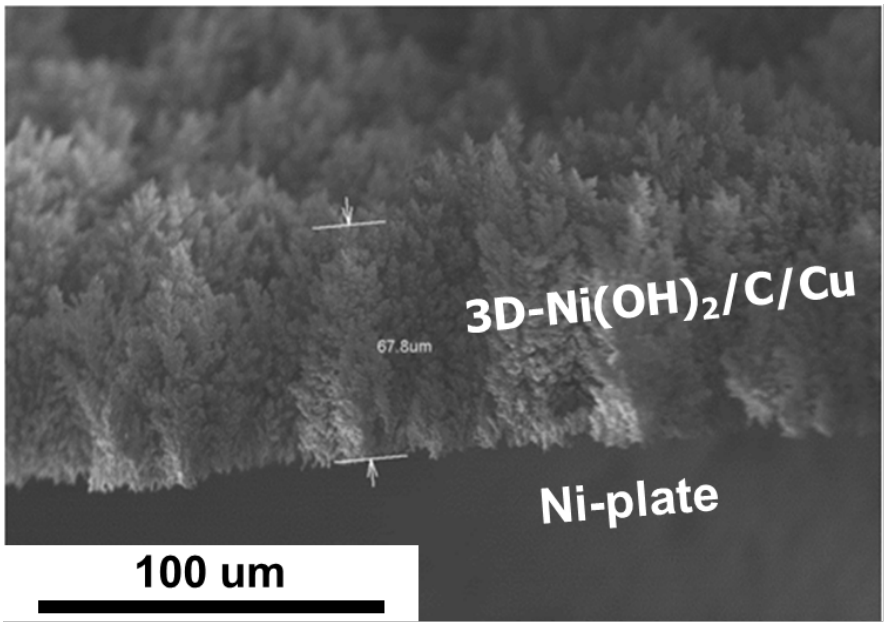

Figure S5. SEM cross section image of the as-synthesized 3D-$Ni(OH)_2$/C/Cu.

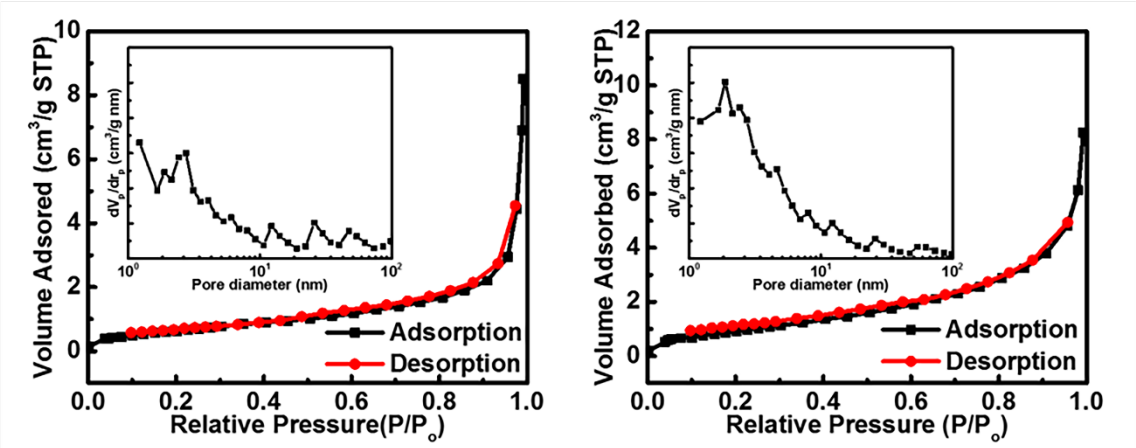

	Surface area (m^2/g)	Pore volume (cm^3/g)	Mean pore size (nm)
3D-C/Cu	2.47	0.012	19.54
3D-$Ni(OH)_2$/C/Cu	4.87	0.009	7.08

Figure S6. The BET data of the 3D-C/Cu and 3D-$Ni(OH)_2$/C/Cu electrode. In the table, comparisons of specific surface area, pore volume and mean pore size are shown in detail.

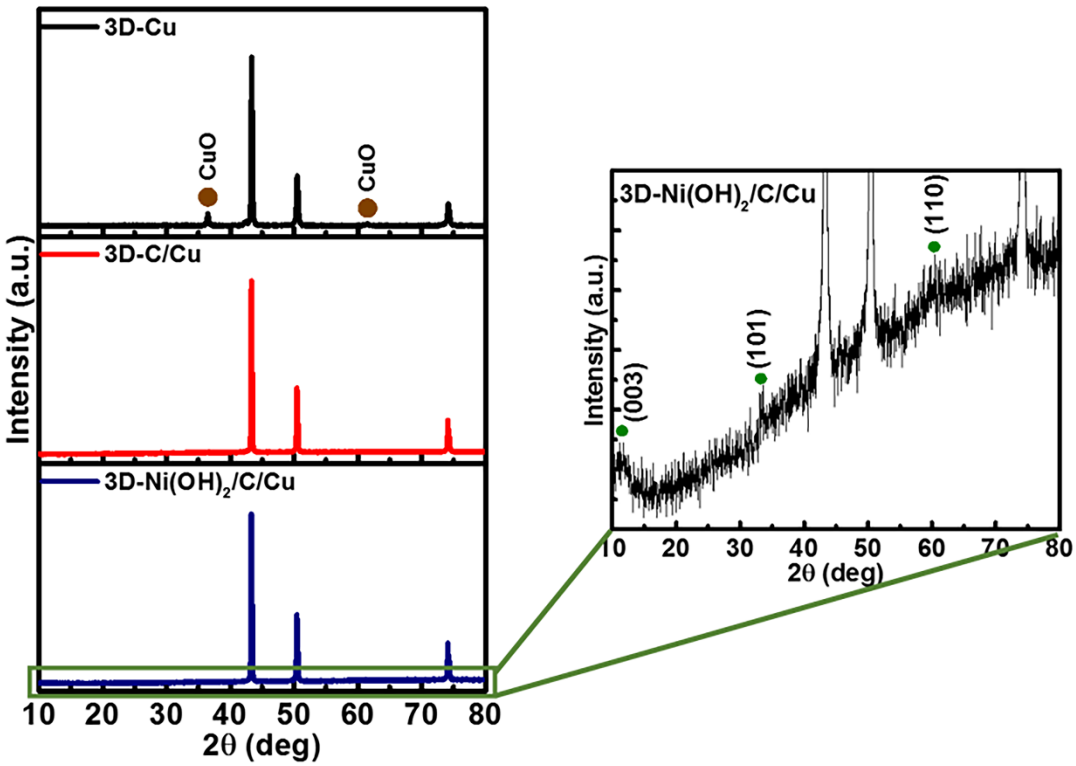

Figure S7. Comparison of XRD patterns of 3D-Cu, 3D-C/Cu, and 3D-Ni(OH)$_2$/C/Cu to determine whether the 3D-Cu structure is oxidized or not (left). Enlarged XRD patterns of the 3D-Ni(OH)$_2$/C/Cu to confirm Ni(OH)2 exactly.

The 3D-Cu XRD pattern (top) shows that Cu and CuO co-exist, because Cu is easily oxidized in air. The peaks at 43°, 51°, and 74° correspond to the (111), (200), and (220) crystalline faces of Cu, respectively, whereas the peaks at 37°, 62° correspond to the (002), (113) planes of CuO. After the carbon coating, 3D-C/Cu XRD patterns didn't show any peak related to CuO. The peaks at 12.1°, 33.4°, 59.8°, corresponding to the (003), (101), (110) planes of Ni(OH)$_2$ in the 3D-Ni(OH)$_2$/C/Cu XRD patterns (bottom) are very weak because the intensity of Cu is much stronger than the thin layer of carbon and Ni(OH)$_2$.

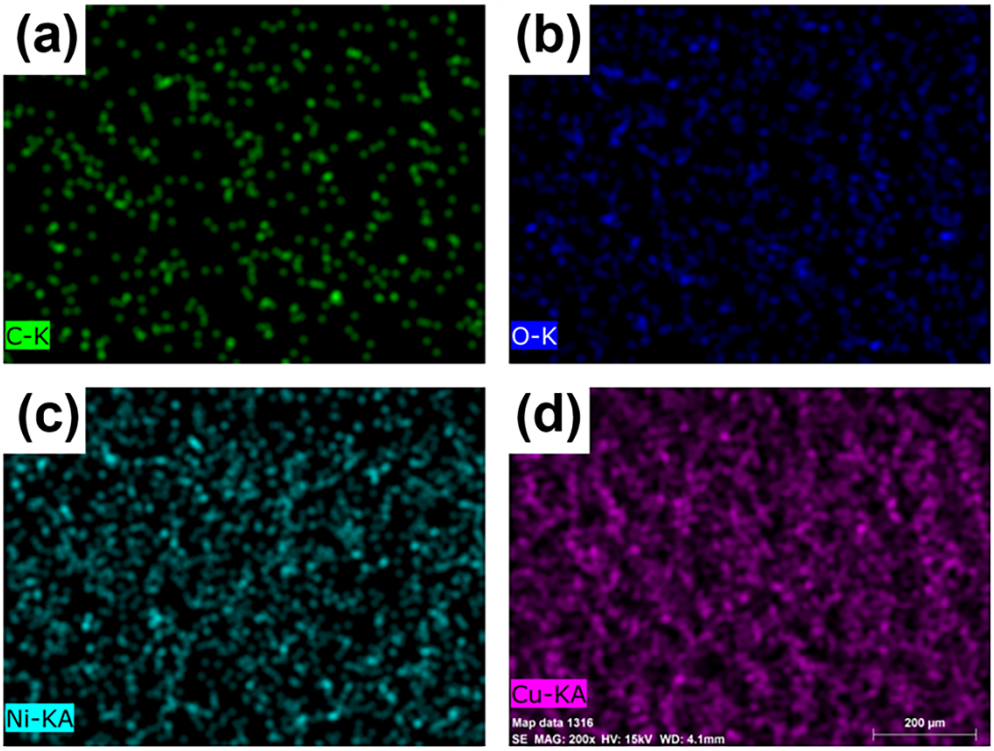

El	AN	Series	Unn.C [wt,%]	Norm.C [wt,%]	Atom.C [at,%]	Error(1 sigma) [wt,%]
C	6	K-series	3.72	2.56	11.48	0.98
O	8	K-series	2.97	2.04	6.87	0.62
Ni	28	K-series	16.36	11.26	10.33	0.61
Cu	29	K-series	122.29	84.14	71.32	4.01
		Total:	145.34	100.00	100.00	

Figure S8. Total EDS elemental mapping images of the as-prepared 3D-$Ni(OH)_2$/C/Cu electrode. And the detail peaks for (a) C, (b) O, (c) Ni and (d) Cu. The table of ratios of all elements, respectively.

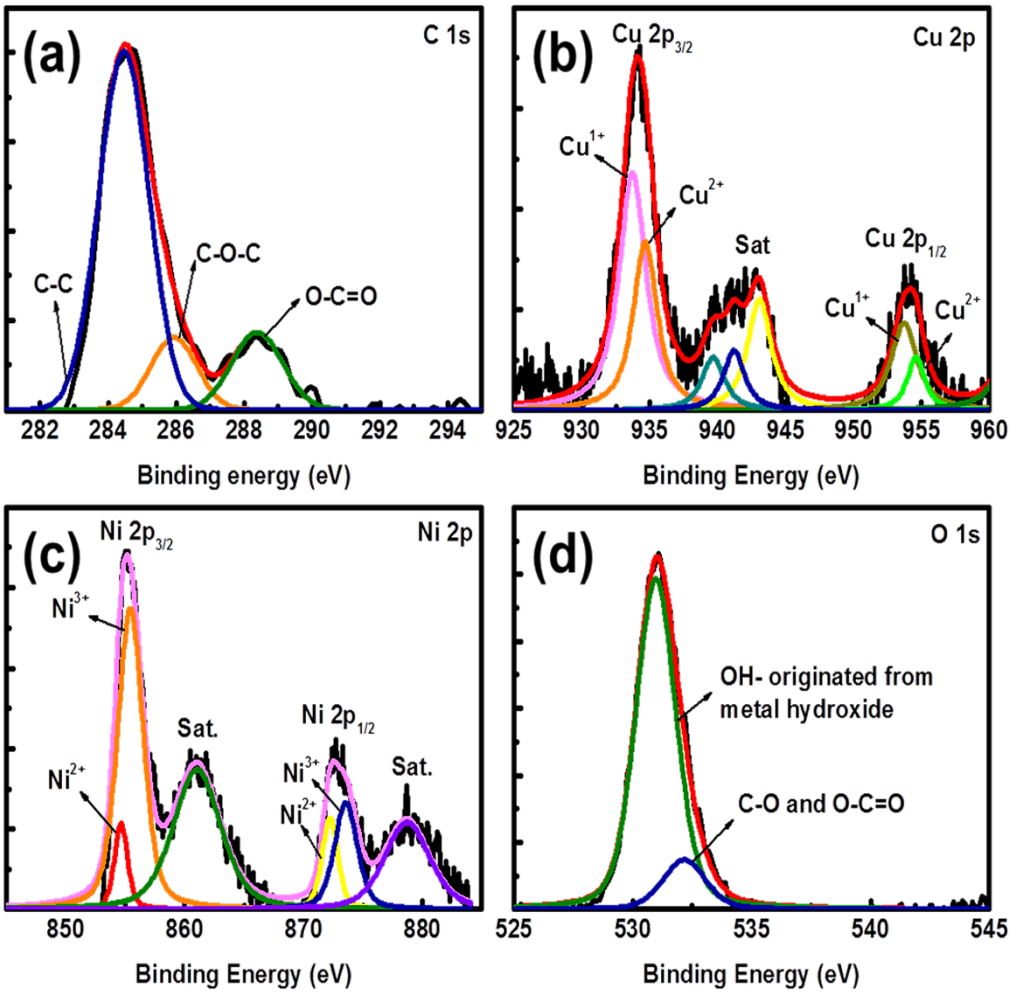

Figure S9. XPS spectra of (a)C 1s, (b) Cu 2p, (c) Ni 2p, and (d) O 1s for the 3D-$Ni(OH)_2$/C/Cu electrode.

In order to further confirm the chemical composition of 3D-$Ni(OH)_2$/C/Cu, XPS (X-ray Photoelectron Spectroscopy) was examined to investigate the electronic state of the elements in the near surface region. Figure S9a shows the C 1s peak, which can be deconvoluted into three peaks corresponding to C-C, C-O and O-C=O moieties. The binding energy at 284.5 eV is originated from the carbon coating layer on 3D-Cu created by annealing the glucose layer. The XPS spectrum of the Cu 2p region of the electrode is shown in Figure S9b. The peaks centered at 934.1 eV and 954.2 eV correspond to $Cu2p_{3/2}$ and $Cu2p_{1/2}$, respectively. The existence of satellite peak in the spectrum suggests the presence of copper in the electrode as Cu(II). The Ni 2p peak at the binding energy at 943 eV as shown in Figure S9c was best fitted with two spin orbit doublets, which are characteristic of Ni^{2+} and Ni^{3+}, and two shakeup

satellites (indicated as "Sat."). Two major peaks with binding energies at 855.2 and 872.6 eV correspond to Ni $2p_{3/2}$ and Ni $2p_{1/2}$, respectively, yielding a spin-energy separation of 17.4 eV, characteristic of the $Ni(OH)_2$ phase. O 1s spectrum in Figure S9d is deconvoluted into two major peaks. One of the major peaks correspond to OH- originated from $Ni(OH)_2$ and other peaks which is related with C-O and O-C=O bonding inherited from carbon source are at 531.5, and 532.5 eV, respectively. The peak at 531.7 eV that is assigned to O 1s photoelectrons, consisting of two oxygen bonds (531.5 eV and 523.5 eV), which can be associated with chemi-absorbed $Ni(OH)_2$ and the abrupt augmentation of single or double bonding between C and O.

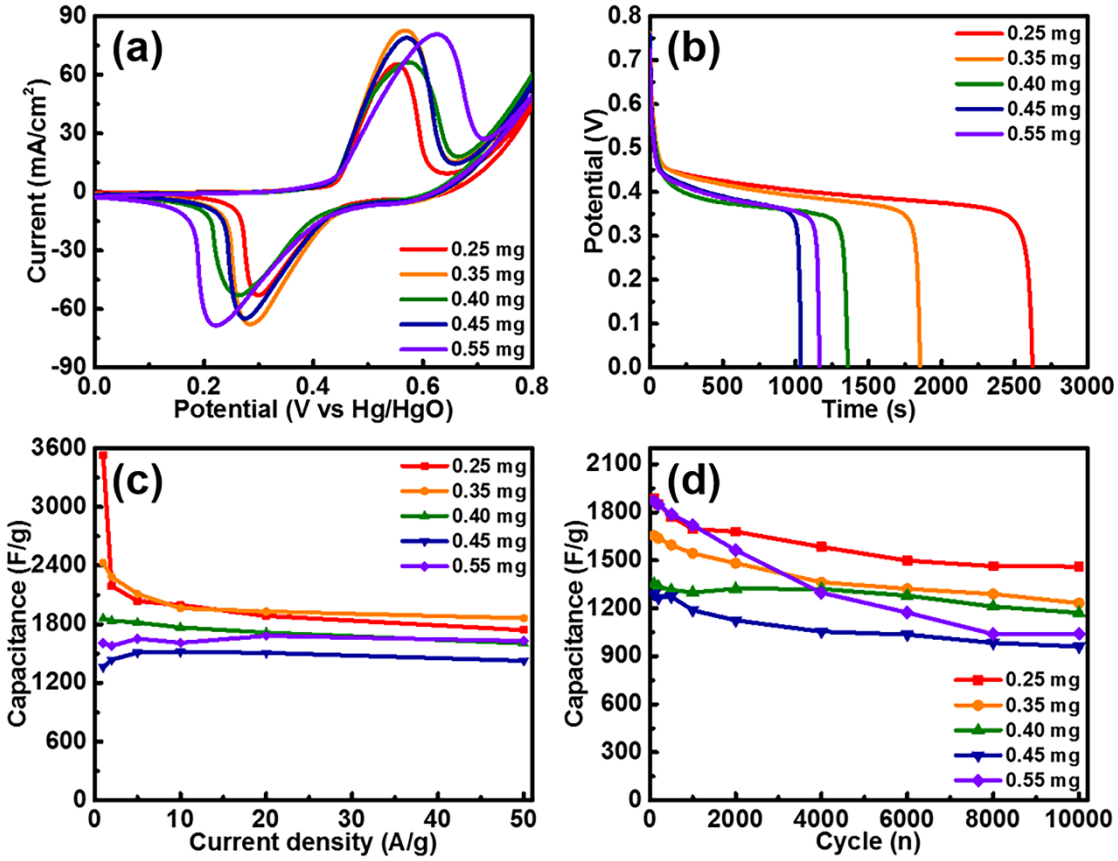

Figure S10. Three-electrode electrochemical measurements of the 3D-$Ni(OH)_2$/C/Cu composite in a 1 M KOH aqueous solution with various amounts of $Ni(OH)_2$. (a) CV curves for different amounts of $Ni(OH)_2$ deposited at 20 mV/s. (b) Galvanostatic charge/discharge curves at 1 A/g, (c) Specific capacitance as a function of the current density. (d) Cycling performance at 200 A/g.

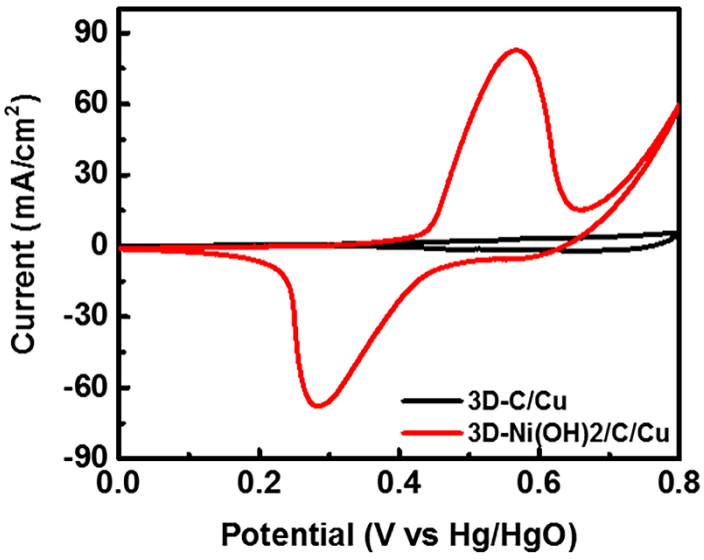

Figure11. Comparison of CV curves between 3D-C/Cu (Current collector) and 3D-$Ni(OH)_2$/C/Cu electrode.

As can be seen in the CVs of 3D-C/Cu and 3D-$Ni(OH)_2$/C/Cu measured at a scan rate 20 mV/s, the current response of 3D-C/Cu (current collector only) is negligible compared to that of 3D-$Ni(OH)_2$/C/Cu. Therefore, we obtained the capacitance value of 3D-$Ni(OH)_2$/C/Cu by considering only the mass of $Ni(OH)_2$.

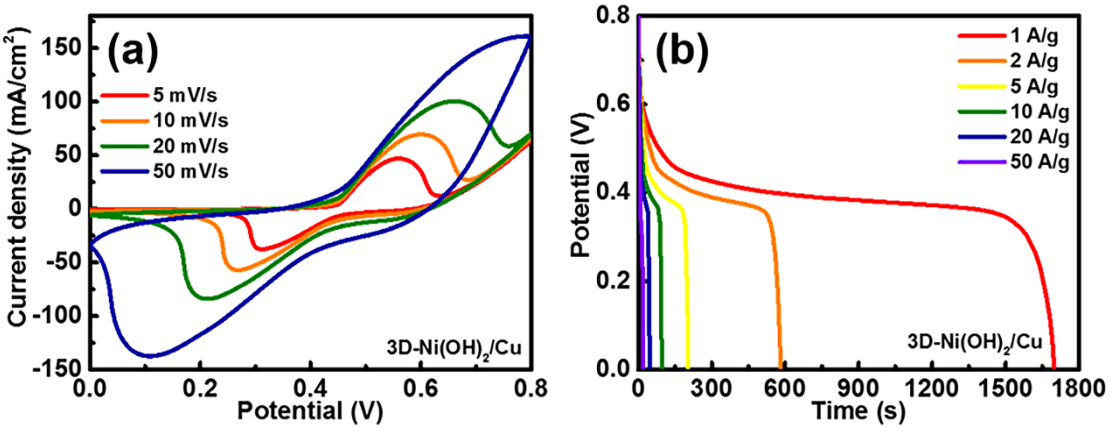

Figure S12. Three-electrode electrochemical measurements of the 3D-$Ni(OH)_2$/Cu composite in a 1 M KOH aqueous solution. (a) CV curves at various scan rates, (b) discharge curves during galvanostatic charge/discharge measurement.

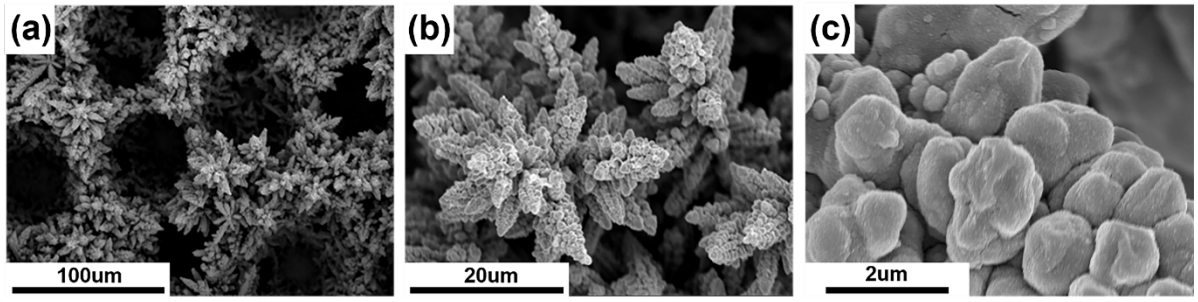

Figure S13. SEM images of (a-c) show the 3D-Ni(OH)$_2$/C/Cu structure after 10000 cycles.

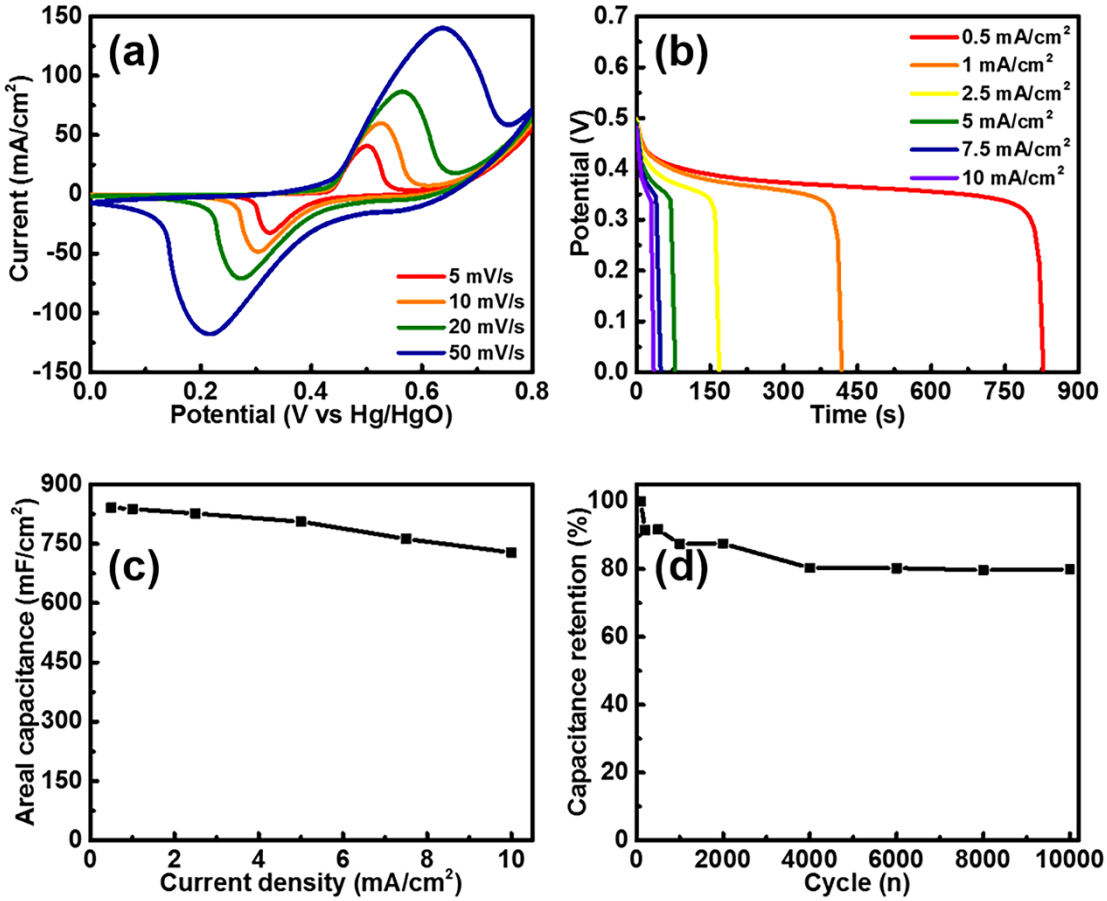

Figure S14. Three-electrode electrochemical performance of the 3D-Ni(OH)$_2$/C/Cu composite in 1 M KOH aqueous solution, for measuring areal capacitance. (a) CV curves of the electrode at different scan rates. (b) Discharge curves of the electrode at different current densities per area. (c) Gravimetric areal capacitance as a function of the current densities, and (d) cycling performance at 20 A/g for 10000 cycles.

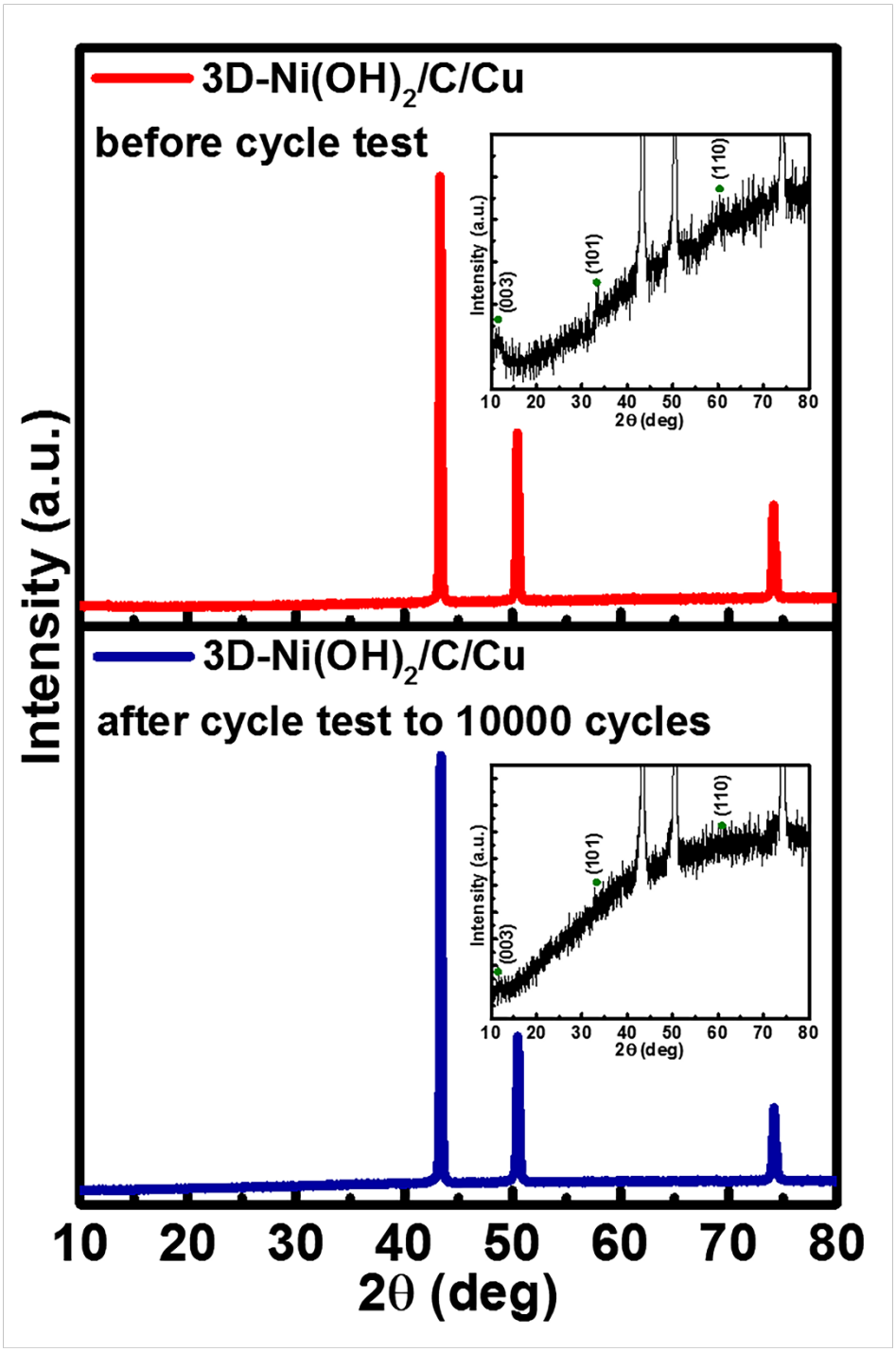

Figure S15. Comparison of XRD patterns of the 3D-Ni(OH)$_2$/C/Cu before and after 10,000 cycles.

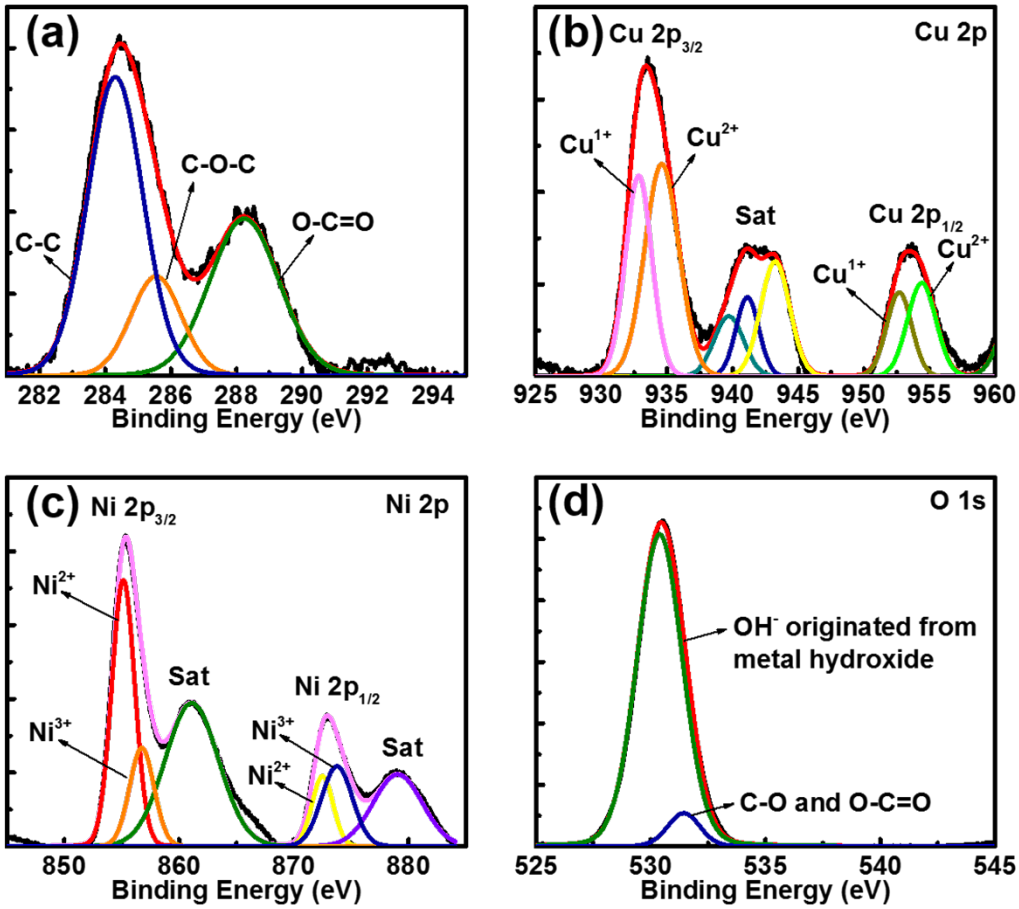

Figure. S16. XPS spectra of (a)C 1s, (b) Cu 2p, (c) Ni 2p, and (d) O 1s for the 3D-$Ni(OH)_2$/C/Cu electrode after 10,000 cycles.

Table S1. Comparison of electrochemical performance of 3D-$Ni(OH)_2$/C/Cu in a three-electrode system with electrodes in other previous paper.

Electrode	Cs (F/g)	Rate capability	Cycle stability	DOI
Amorphous $Ni(OH)_2$ nanospheres on nickel film	2188 (at 1 mV/s)	43 % (1 mV/s to 20 mV/s)	72 % 10000 cycles	10.1038/ncomms2932 [27]
$Ni(OH)_2$ nanoplates grown on graphene	1335 (at 2.8 A/g)	70 % (2.8 A/g to 45.7 A/g)	Almost 100 % (20000 cycles)	10.1021/ja102267j [28]

α-$Ni(OH)_2$ on nickel foam	3152 (at 4 A/g)	8.9 % (4 A/g to 16 A/g)	48 % (3000 cycles at 4 A/g)	10.1039/B815647F [29]
Ultrathin $Ni(OH)_2$ nanosheet on nickel foam	2384.3 (at 1 A/g)	54 % (1 A/g to 4 A/g)	75 % (3000 cycles at 5 A/g)	10.1016/ j.nanoen.2014.10.029 [30]
Nanoporous $Ni(OH)_2$ thin film on 3D ultrathin graphene foam	1560 (at 0.5 A/g)	70 % (0.5 A/g to 10 A/g)	65 % (1000 cycles at 10 A/g)	10.1021/nn4021955 [26]
3D-$Ni(OH)_2$/C/Cu on Ni film_0.35 mg	2430 (at 1 A/g)	76.7 % (1 A/g to 50 A/g)	74.5 % (10000 cycles at 200 A/g)	This work
3D-$Ni(OH)_2$/C/Cu on Ni film_0.40 mg	1860 (at 1 A/g)	86.3 % (1 A/g to 50 A/g)	86.5 % (10000 cycles at 200 A/g)	This work

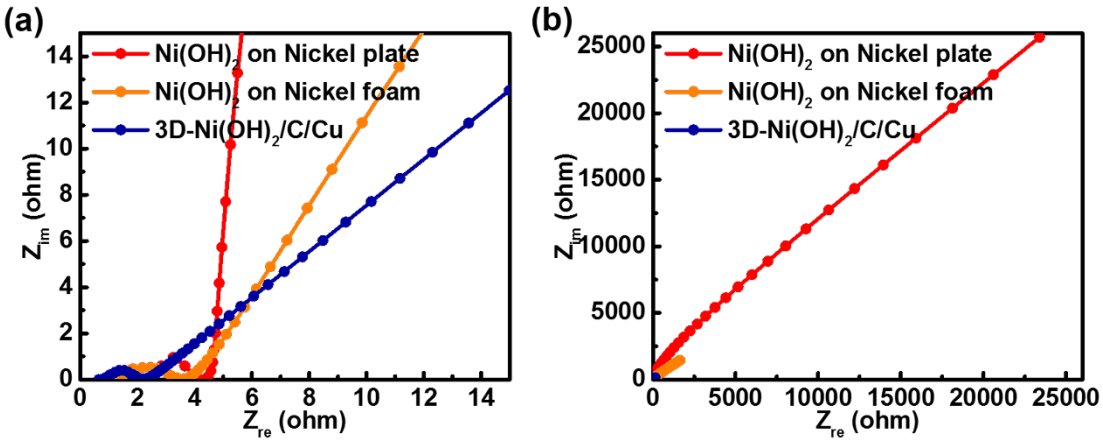

Figure S17. Zoom-up range (a) and gauge span (b) of EIS of the as-prepared electrode (blue) and other references : $Ni(OH)_2$ on nickel film, and $Ni(OH)_2$ on nickel foam.

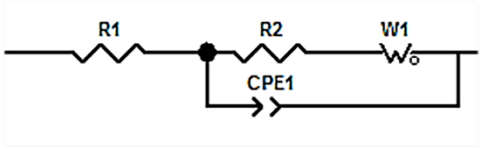

R1 (R_s) : Cell internal resistance
R2 (R_{ct}) : Charge transfer resistance
CPE 1 : Double layer capacitance
W1 : Warburg element

	3D-Ni(OH)$_2$/C/Cu	3D-Ni(OH)$_2$/Cu
R1 (R_s)	0.65Ω	0.48Ω
R2 (R_{ct})	0.65Ω	0.74Ω

Figure S18. Model and values of Electrochemical Impedance Spectroscopy (EIS) of the 3D-Ni(OH)$_2$/Cu and 3D-Ni(OH)$_2$/C/Cu electrodes.

For an asymmetric cell

For a supercapacitor, the charge balance will follow the relationship $q_+ = q_-$. The charge stored by each electrode depends on the specific capacitance (C), the potential range for charge/discharge (△E) and the mass of the electrode (m) following the equation. Q = C x△E x m and in order to get $q_+ = q_-$, the mass balancing will follow the equation $\frac{m_+}{m_-} = \frac{C_- \, x \, \Delta E}{C_+ \, x \, \Delta E}$.

On the basis of the specific capacitance values and potential windows found for the 3D-Ni(OH)$_2$/C/Cu and AC, the optimal mass ratio between the electrodes should be m(3D-Ni(OH)$_2$/C/Cu)/m(AC) = 0.148 in the asymmetric supercapacitor cell. In the 1cm^2 electrode, an optimal AC loading mass is difficult to achieve due to above mass ratio between the cathode and anode. So, we deposited a 1:4 ratio of Ni(OH)$_2$ and AC and measured it, as shown in Figure S15.

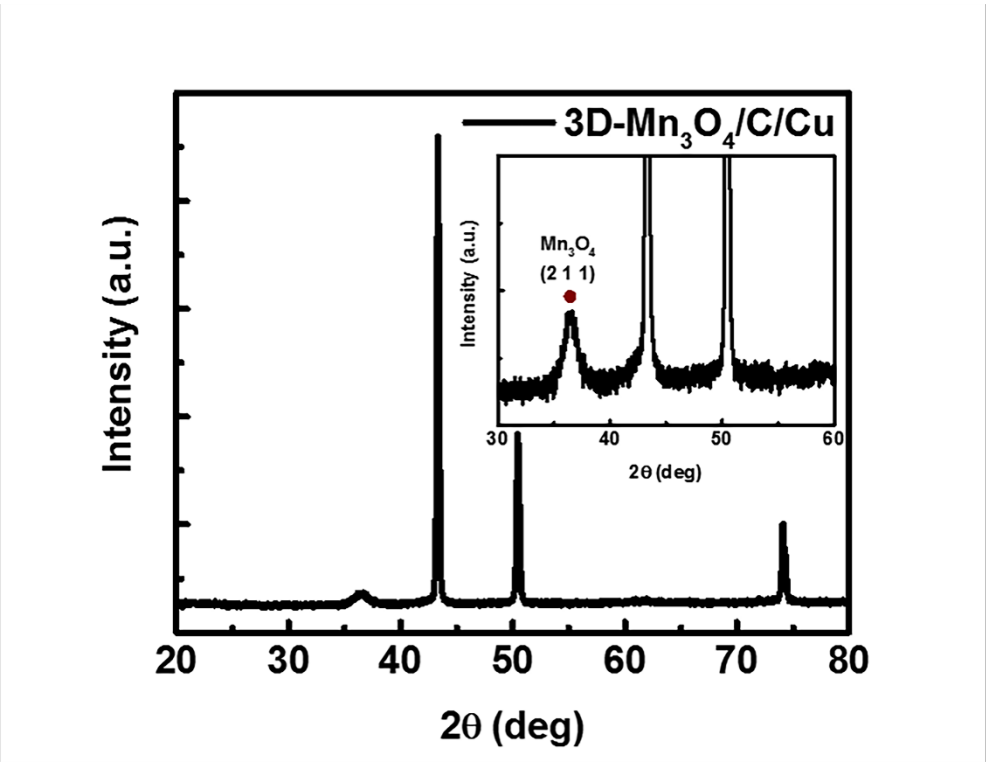

Figure S19. XRD patterns of 3D-Mn_3O_4/C/Cu. The inset shows enlarged XRD patterns of 3D-Mn_3O_4/C/Cu.

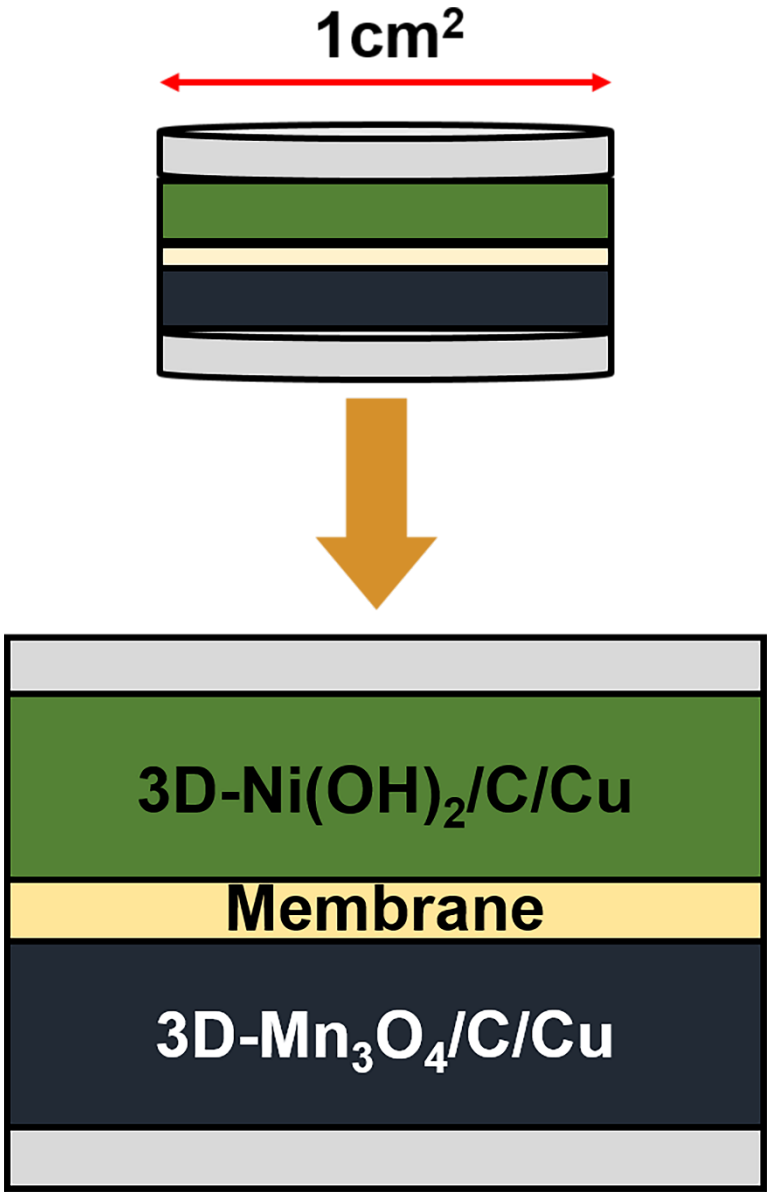

Figure S20. Schematic illustration of the assembled 3D-$Ni(OH)_2$/C/Cu//3D-Mn_3O_4/C/Cu devices.

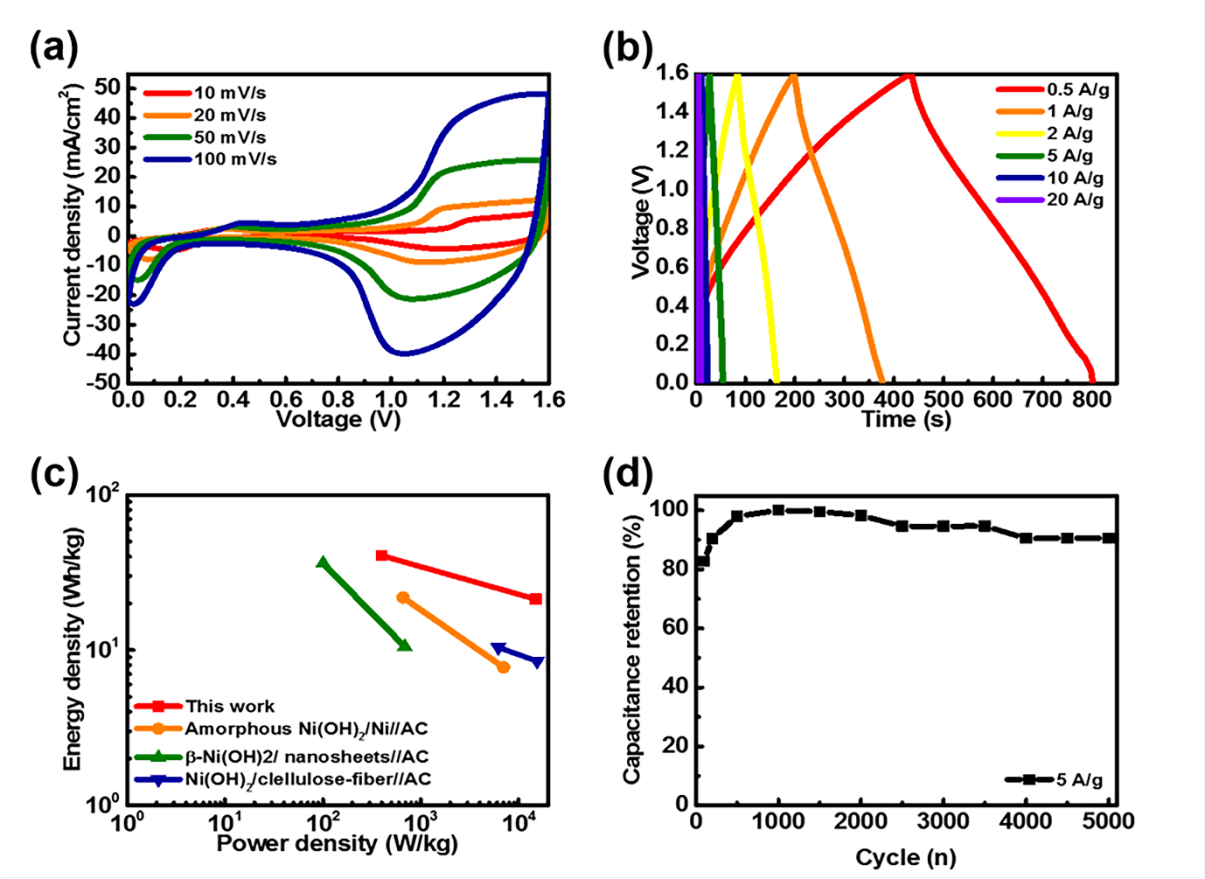

Figure S21. (a) CV curves of the 3D-$Ni(OH)_2$/C/Cu//Activated carbon asymmetric supercapacitor measured at different scan rates of 10, 20, 30, 40, and 50 mV/s between 0 and 1.6 V in 1 M KOH aqueous electrolyte, (b) Galvanostatic charge/discharge curves of the 3D-$Ni(OH)_2$/C/Cu //Activated carbon asymmetric supercapacitor as a function of different current densities, (c) Ragone plot of the 3D-$Ni(OH)_2$/C/Cu with other references and (d) specific capacitance retention of the 3D-$Ni(OH)_2$/C/Cu //Activated carbon asymmetric supercapacitor as a function of cycle.

The rectangular shaped CV curve of the activated carbon electrode indicates an electric double layer capacitance, whereas the distorted CV curve of the 3D-$Ni(OH)_2$/C/Cu reveals a pseudocapacitance behavior in addition to the double layer effect. Because activated carbon and 3D-$Ni(OH)_2$/C/Cu can store electric charges between the potential windows of -1.0 V and 0.6 V vs Hg/HgO, respectively, the asymmetric supercapacitor designed from these electrodes can operate from 0 to 1.6 V. Because the maximum achievable potential windows of the electrodes using unit masses are estimated from the corresponding CV plots, the appropriate

mass loadings of the electrode materials can be determined to design an asymmetric supercapacitor with the highest performance. Figure 5b show the galvanostatic charge-discharge curves of the electrode at constant current densities of 0.5, 1, 2, 5, 10, and 20 A/g, within the potential window of 0-1.6 V. The nonlinear charge-discharge plots further support the fast and reversible redox peaks recorded in the CV plots. The specific capacitance calculated from the discharge curve is 366.8 F/g at a constant current of 0.5 A/g, which is superior to that of similar $Ni(OH)_2$ electrodes.[1-3]

1. Su, Y.-Z.; Xiao, K.; Li, N.; Liu, Z.-Q.; Qiao, S.-Z., Amorphous Ni(OH)2@ three-dimensional Ni core–shell nanostructures for high capacitance pseudocapacitors and asymmetric supercapacitors. *Journal of Materials Chemistry A* **2014,** *2* (34), 13845.

2. Huang, J.; Xu, P.; Cao, D.; Zhou, X.; Yang, S.; Li, Y.; Wang, G., Asymmetric supercapacitors based on β-Ni(OH)2 nanosheets and activated carbon with high energy density. *Journal of Power Sources* **2014,** *246*, 371-376.

3. Zhang, L.-L.; Li, H.-H.; Fan, C.-Y.; Wang, K.; Wu, X.-L.; Sun, H.-Z.; Zhang, J.-P., A vertical and cross-linked Ni(OH)2network on cellulose-fiber covered with graphene as a binder-free electrode for advanced asymmetric supercapacitors. *J. Mater. Chem. A* **2015,** *3* (37), 19077-19084.